Gold Coating of Silver Nanoprisms

*Mohammad Mehdi Shahjamali, Michel Bosman, Shaowen Cao, Xiao Huang, Somaye Saadat, Erik Martinsson, Daniel Aili, Yee Yan Tay, Bo Liedberg, Say Chye Joachim Loo, Hua Zhang, Freddy Boey, and Can Xue**

Core–shell Ag@Au nanoprisms are prepared through a surfactant-free seed-mediated approach by taking advantage of the anisotropic structure of silver nanoprisms as seeds. The gold coating on the silver nanoprism surface is achieved by using hydroxylamine as a mild reducing agent, and the final fully gold-coated prism structures are confirmed by microscopic and spectroscopic characterization. The resulting Ag@Au core–shell structure preserves the optical signatures of nanoprisms and offers versatile functionality and particularly better stability against oxidation than the bare silver nanoprism. The surface plasmon resonances of the core–shell Ag@Au nanoprisms can be tuned throughout the visible and near-IR range as a function of the Au shell thickness. Such tailorable optical features and surfactant-free gold shells have great potential applications in biosensing and bioimaging.

1. Introduction

Shape-controlled nanostructure synthesis of noble metals, such as silver and gold in particular, has attracted a great deal of attentions in recent years because of the unusual optical properties of noble metal nanostructures, which are known as localized surface plasmon resonance (LSPR),[1–4] as well as their novel chemical,[5] electronic,[6] and catalytic properties.[7] Thereby a broad range of intriguing applications emerges in the field of photonics,[8] catalysis,[9] biological and chemical sensing,[5,10] surface-enhanced Raman scattering (SERS),[11,12] metal-enhanced fluorescence (MEF),[13–15] and energy conversion.[16,17]

The need to produce nanoparticles (NPs) with finely tuned optical properties has therefore led to enormous research efforts to develop reliable routes to synthesize noble metal NPs with controllable shapes and sizes. To tailor the nanoparticle properties and improve their performance in various applications, people have developed many chemical methods for generating Au and Ag nanocrystals with a rich variety of shapes, including sphere,[18] rod,[19] wire,[20] prism,[21,22] cube,[23] octahedron,[24] star,[25] icosahedron,[23,26] and bipyramid.[27]

Bimetallic Ag and Au nanocrystals are particularly attractive because they possess a broader range of plasmon tunability and versatile surface functionalities than does the individual unit of a Ag or Au nanocrystal. By combining Au and Ag into core–shell structures, the LSPR signatures of these nanosturctures can be controlled not only by varying the size and shape of the core but also the shell thickness.[4,28] The close lattice match between Au and Ag (<0.3% mismatch) plays a key role in achieving conformal epitaxial growth. For example, Au@Ag core–shell nanocrystals with various morphologies have been synthesized through an epitaxial growth process involving conformal Ag deposition on the surface of Au seeds.[29,30]

However, the formation of a structure with an Ag core and an Au shell remains challenging due to the significant etching of Ag cores by Au salt precursors, which is known as galvanic replacement and typically leads to the generation of nanoframes,[31] or hollow nanoboxes,[32] or other irregular nanoparticles with random optical responses. In particular, when the core is a very thin silver prism (<10 nm), the tip is so vulnerable to oxidation that the flat (111) faces tend to be preferentially etched through the galvanic process. For example, by seeding with Ag nanoplates, Zou et al. produced bimetallic Ag–Au nanostructures with nonuniform gold coating and pinholes in the structure.[33] Sanedrin et al. reported rounded-tip triangular Ag@Au core–shell structures with corrugated gold shells by using cetyltrimethylammonium bromide (CTAB) as the surfactant to mitigate Ag prism etching.[34] However, the presence of CTAB led to severe tip truncation of the Ag prism cores. More seriously, the strong passivation of gold shell surfaces by CTAB induces tremendous difficulties when further surface modification is needed for application purposes.

Although the vulnerablility of these thin nanostructures makes the shape-controlled gold-coating process extremely challenging, targeting a nanostructure with an Ag nanoprism core and controllable Au shell thickness is very attractive since the SPR wavelength of Ag nanoprisms can be finely tuned through

M. M. Shahjamali, Dr. S. W. Cao, Dr. X. Huang, S. Saadat, Dr. Y. Y. Tay, Prof. S. C. J. Loo, Prof. H. Zhang, Prof. F. Boey, Prof. C. Xue
School of Materials Science and Engineering
Nanyang Technological University
50 Nanyang Avenue, 639798, Singapore
E-mail: cxue@ntu.edu.sg
Dr. M. Bosman
Institute of Materials Research and Engineering
A*STAR, 3 Research Link, 117602, Singapore
E. Martinsson, Prof. D. Aili, Prof. B. Liedberg
Division of Molecular Physics
Department of Physics
Chemistry and Biology
Linköping University
SE-581 83 Linköping, Sweden

DOI: 10.1002/adfm.201102028

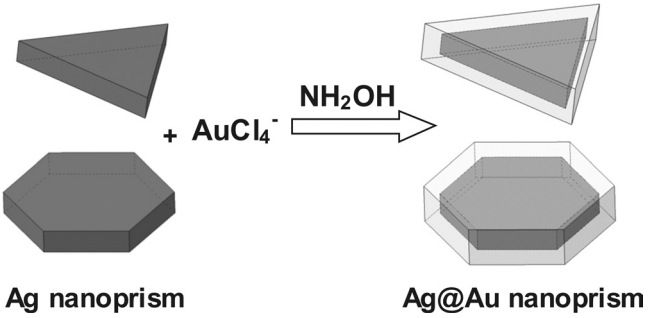

Scheme 1. Schematic illustration of the gold coating process of silver nanoprisms.

the entire visible spectrum and even part of the near-IR range. The ideal gold coating would provide significantly enhanced stability and allow the full functionalities of gold surfaces to enable wide application. Herein we report a straightforward method for gold coating of Ag nanoprisms while retaining the shape of triangular Ag cores (**Scheme 1**). Electron microscopic analysis is used to confirm the formation of gold layers on all facets of the Ag nanoprism seeds, which leads to a core–shell structure that preserves the optical features of Ag nanoprisms and offers better stability against oxidation and more versatile functionalities than bare Ag nanoprisms. We also systematically investigate how the controlling parameters, such as reagent concentration, pH value, and infusion rate, influence the gold coating process.

2. Results and Discussion

2.1. Gold Coating Process of Ag Nanoprisms

Herein, the main goal is to utilize readily available reagents to coat Ag nanoprisms with a thin layer of gold, while preserving prism shape and minimizing the Ag prism etching by gold precursor ions ($AuCl_4^-$ and $AuCl_2^-$). We use a straightforward seed-mediation approach that involves hydroxylamine (HyA) to reduce the gold salt. The reaction is very mild to ensure epitaxial gold growth on the Ag nanoprism and also to guarantee that the reduction of gold salts only occurs on the surface of Ag nanoprism seeds and spontaneous nucleation of gold NPs is avoided. In addition, it is notable that HyA exhibits little etching of silver and gold nanocrystals when compared with other mild reducing agent such as ascorbic acid, which has been reported to show etching on silver nanoprisms,[35] and gold nanorods.[36]

Table 1. Different experimental stages of the gold coating process.

Stage	Duration of stage [min]	Rate [mL h^{-1}]	Reducing agent	[$HAuCl_4$] [mM]
1	0–30	1.00	Standard NH_2OH•HCl	0.2748
2	30–120	1.00	Basic NH_2OH•HCl	0.2748
3	120–135	3.00	Standard NH_2OH•HCl	0.2748
4	135–200	1.00	3× Standard NH_2OH•HCl	3 × 0.2748

The gold coating process was carried out by slowly introducing $HAuCl_4$ and HyA simultaneously into the Ag nanoprism solution through two separate tubes on a mechanical syringe pump. Throughout the whole process, the solution was kept under vigorous magnetic stirring. The synthetic route has four different stages as summarized in **Table 1**. Since the reducing power of hydroxylamine is enhanced at higher pH values,[33] in stage 2 we introduced some NaOH into the hydroxylamine solution to increase pH and boost the gold deposition rate. As the LSPR bands of gold and silver NPs are highly sensitive to changes in their size and shape, we are able to track and evaluate the structure evolution during the coating process based on the extinction spectra of the NPs. To monitor the gold coating process, an aliquot of the solution was taken at 15-min intervals during the reaction for characterization by UV-Vis spectroscopy and transmission electron microscopy (TEM).

Figure 1 indicates that in the first stage the LSPR band redshifts and increases in intensity with time. This result corresponds to an initial Au deposition on the Ag prism edges, which makes the edges show up with greater contrast under TEM observation (**Figure 2**b). This deposition is due to the high surface energy of the (110) planes on the Ag prism edges, so that

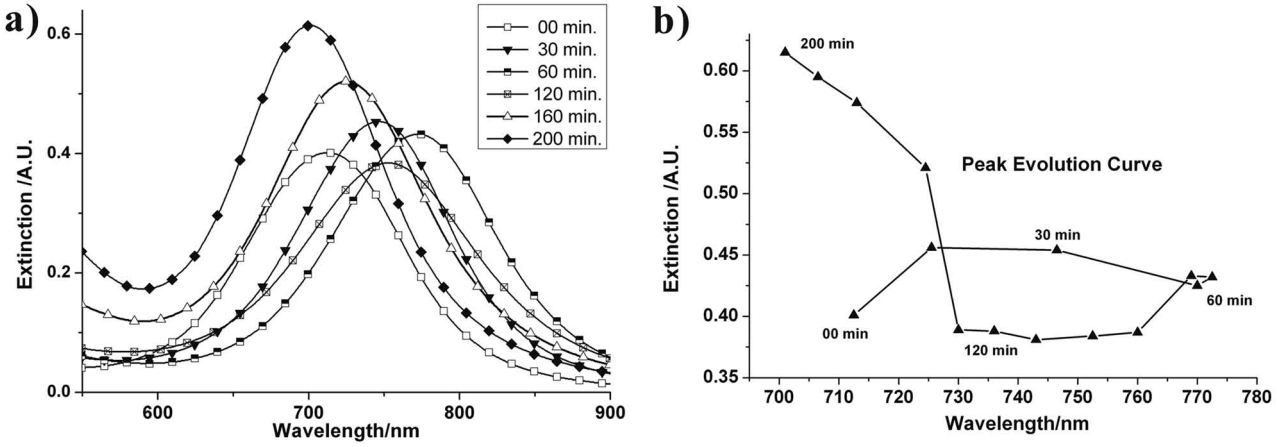

Figure 1. UV-Vis extinction spectra during the gold coating process. a) Spectra of samples from 0 to 200 minutes. b) Peak evolution curve of A (each point of this diagram corresponds to λ_{max} of the solution at a different time).

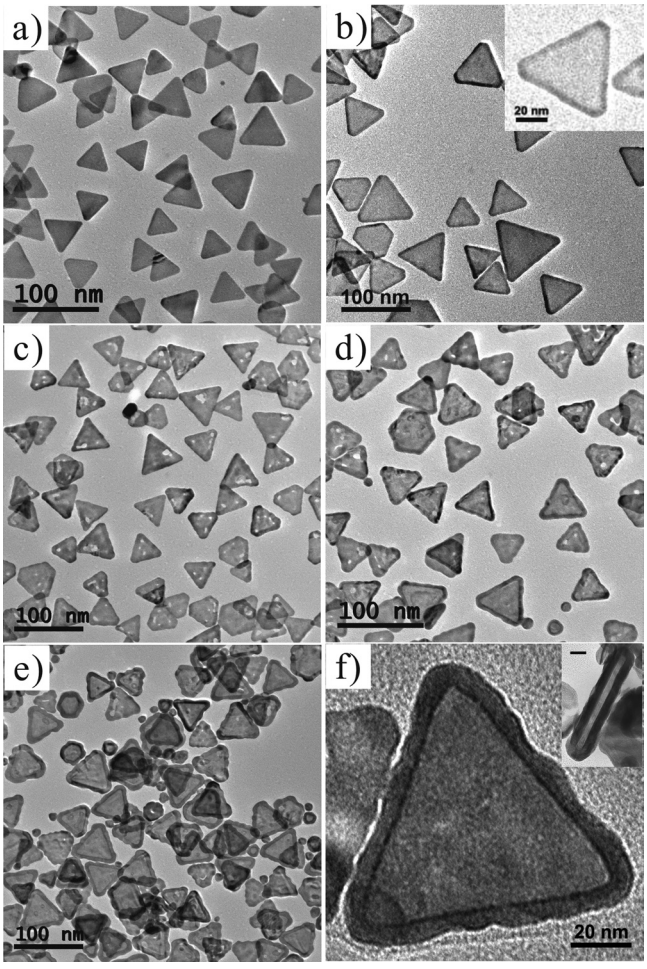

Figure 2. TEM images of a) initial silver nanoprisms; b) samples at 45 min with gold deposition on the prism edges; c) samples from stage 2 with some small pinholes; d) samples with partially refilled pinholes after 120 min (stage 3); e) samples at 200 min with full gold shells (stage 4); f) a typical final gold-coated nanoprism (the inset is the cross-sectional view with a scale bar of 10 nm).

gold atoms deposit preferentially on these sites. A further red-shift of the LSPR band with dampening intensity is attributed to (111) face etching of Ag prisms by $HAuCl_4$.[35] Consistently, Figure 2c shows that some areas on the triangular surface exhibit less contrast and small pinholes appear in the prism structure. This etching process is known as galvanic replacement, and it preferentially occurs on the (111) plane when the gold salt concentration reaches a certain value. This process indeed reduces the thickness of some areas of the Ag prisms, causing a red-shift of the LSPR band, and eventually creates pinholes while the gold-coated edges remain undamaged.

In stage 3, we observed a progressive blue-shift with increasing intensity of the LSPR band. TEM analysis revealed that the etched areas on the triangular plane are refilled with Au and Ag alloy (Figure 2d), and this process is followed by continuous pure gold deposition towards a fully gold-coated prism structure (Figure 2e–2f). The structure characterization and confirmation will be detailed in Section 2.2. The backfilling process refills the pinholes and recovers the prism thickness,

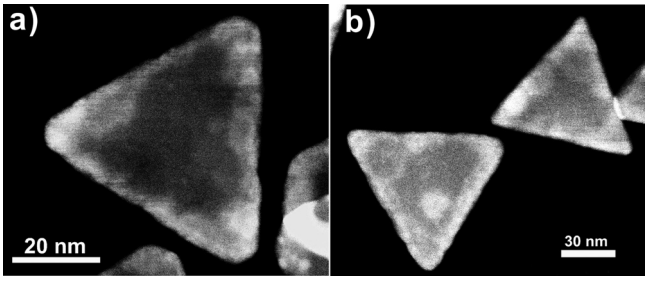

Figure 3. a) HAADF-STEM image at 45 min, showing obvious deposition of gold on the edges of silver nanoprisms. b) HAADF-STEM image at 60 min, showing the deposition of gold on the prism edges with spread into the (111) facet.

which results in a blue-shift of the LSPR band. The steady increase of LSPR intensity indicates that the prism edge length also increases. To obtain a clearer view of the LSPR band correlated with the structural changes at different stages, the evolution of LSPR band during the entire gold coating process is depicted in Figure 1b in terms of peak evolution.

2.2. Structure Analysis of Gold-Coated Silver Nanoprisms

Detailed microscopic analyses were carried out for the product at each growth stage to obtain convincing evidence of the structures. The average edge length and thickness of the Ag nanoprisms before gold deposition were measured as 56 and 6 nm, respectively. At the early stage, when gold starts to deposit on the Ag prism edges, the contrast between Ag and Au may not be clearly distinguishable under normal bright-field TEM mode for some samples (Figure 2b), hence we used the high-angle annular dark-field scanning transmission electron microscopy (HAADF-STEM), where the signal contrast is proportional to the atomic number (Z). The large difference in Z values between Ag (47) and Au (79) allows distinct differentiation of these two elements. As shown in **Figure 3**a, the clear bright edges of the prisms in dark-field mode indicate the Au coating on the edges of the prisms after the first 45 min of the reaction. This gold coating further tends to spread into the center of the triangular plane by 60 min in the coating process (Figure 3b). The energy-dispersive X-ray spectroscopic (EDX) line-scan examinations of the prisms from the side view (**Figure 4**b and c) reveal that the triangle surface consists of both Ag and Au, which suggests that the surface consists of an alloy.

However, the final structure of the gold-coated silver nanoprism exhibits a fully gold-coated surface, as shown in the EDX profile of the edge (Figure 4d). After the coating process, the prism thickness can increase up to 17 nm while the initial thickness is characterized as 6 nm (Figure S2). High-resolution TEM (HRTEM) examination (**Figure 5**) shows that the core–shell structure is still single-crystal and the triangle face is still a (111) plane with a close-packed hexagonal lattice. X-ray photoelectron spectroscopy (XPS) analyses were carried out to further confirm the gold coating. As shown in Figure S4A and S4B, when these core–shell triangular nanocrystals are sputtered with Ar^+ ions, the Au/Ag ratio firstly decreases and

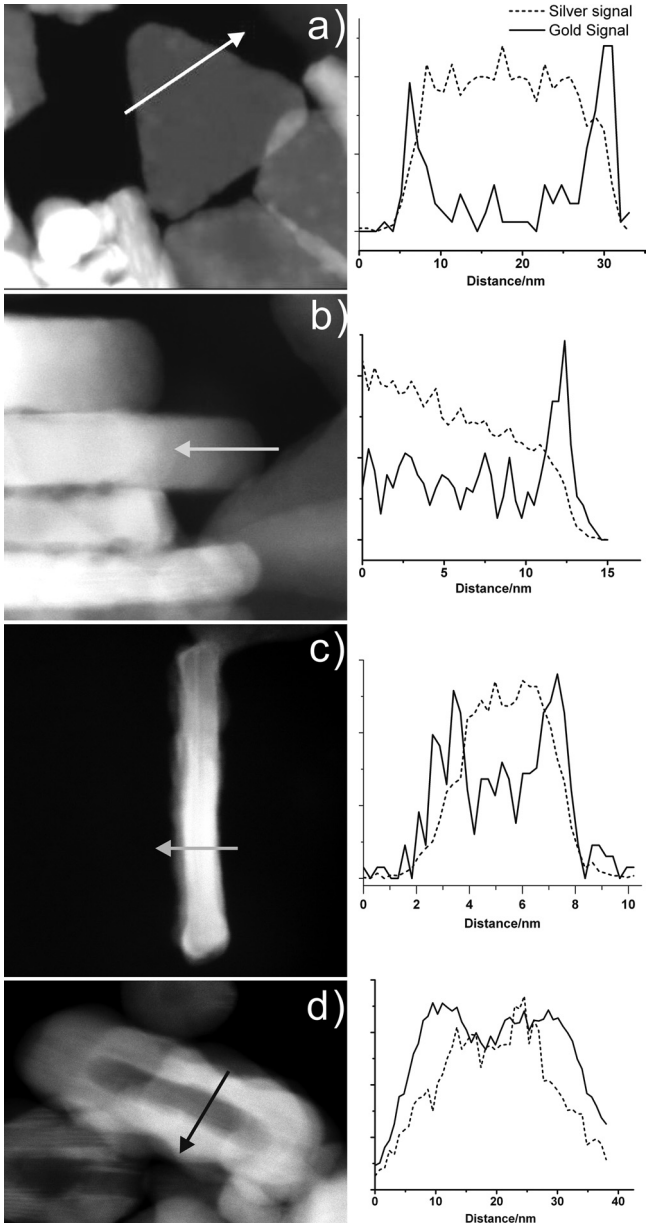

Figure 4. STEM images and EDX line-scan profiles of Ag@Au nanorisms at 60 min (a–c) and 200 min (d).

then increases, which is in accordance with a sandwich morphology of the Ag@Au nanoprisms in the cross-section. This result reinforces the conclusion that we have formed a complete gold coating as the outermost layer of the nanoprism.

2.3. Discussion on the Growth Stages

Based upon the TEM analysis of the samples taken during the gold-coating process, a general trend of morphological changes can be observed for the formation of Ag@Au core–shell nanoprisms. This formation includes four main growth stages:

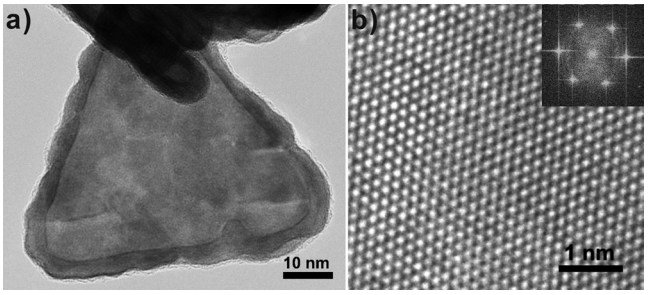

Figure 5. a) TEM image of the Ag@Au core–shell nanoprism. b) HRTEM image taken along a direction perpendicular to the flat top faces. The inset fast Fourier-transformed (FFT) patterns shows six-fold hexagonal symmetry corresponding to the (111) plane.

i) Initial Deposition of Au atoms on the Silver Nanoprism Edges: At the very beginning, the $HAuCl_4$ concentration is too low to induce noticeable etching while the deposition of Au atoms on the Ag nanoprism (110) and (100) facets still proceeds, as the high surface energy of these facets enables effective activation of the reaction between HyA and $HAuCl_4$. The initial Au deposition on the nanoprism edges is similar to the epitaxial Au growth reported by Aherne et al., where formation of a gold layer along the Ag nanoprism edges was observed by using L-ascorbic acid as the reducing agent.[35] Aherne et al. proposed that the initial Au layer deposited onto the Ag nanoprism edges can protect the prism edges against etching by Cl^- and $AuCl_4^-$.[35] The chemical reactions involved in the initial gold coating process are believed to occur as follows (Equations 1 and 2).

$$6NH_3OH^+ \leftrightarrow 6\,e^- + 12H^+ + 6H_2O + 3N_2 \quad (1)$$

$$2\,Au^{3+} + 4\,e^- \rightarrow 2Au^+$$
$$2\,Au^+ + 2\,e^- \rightarrow 2Au^0 \quad (2)$$

ii) Etching of Nanoprism (111) Facets: As the $HAuCl_4$ concentration increases, the (111) facets start to be etched through galvanic corrosion, while the Ag nanoprism edges are protected by the initially deposited Au layers. The etching is due to the difference in the redox potentials between Ag^+/Ag (0.8 V vs. SHE; SHE = standard hydrogen electrode) and $AuCl_4^-/Au$ (0.99 V vs. SHE), which leads to the oxidation of Ag nanoprisms by gold ions.[37] In this stage, if the silver etching rate is uncontrollably fast, some random structures can be observed, including semihollow structures with lots of pinholes (Figure S3A), and small broken pieces of nanoprisms (Figure S3B). This template-engaged replacement reaction could be described according to Equation 3.

$$3Ag\,(s) + AuCl_4^-\,(aq) \rightarrow Au\,(s) + 3Ag^+\,(aq) + 4Cl^-\,(aq) \quad (3)$$

iii) Backfilling of the Etched Pinholes with Ag–Au Alloy: The etched (111) facets of Ag prisms are backfilled with Ag–Au alloy at this stage. In the TEM observation, these nanoprisms often exhibit varied contrast in the backfilled pinhole sites (Figure 2d). The primary reaction observed in the backfilling process is gold deposition onto the inner edges of the pinholes without altering the nanoprism thickness. Hence the backfilling is believed to be face-selective. Due to the large roughness at the inner edges of pinholes, these sites

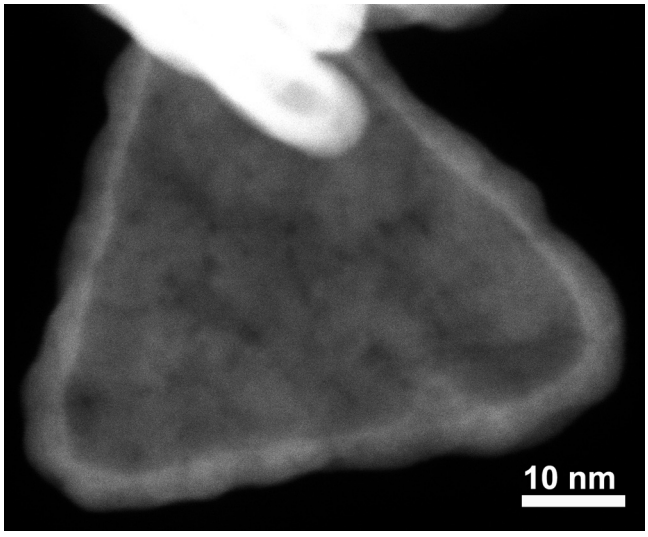

Figure 6. HAADF-STEM image of a fully gold-coated prism at 200 min.

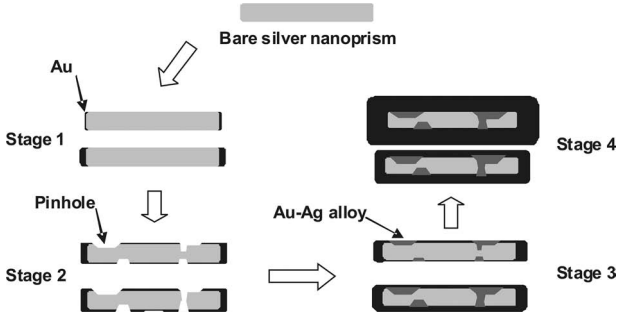

Scheme 2. Schematic illustration of the formation of Ag@Au core–shell nanoprisms,showing a cross-sectional view of a typical growing core–shell Ag@Au nanoprism and the manner of its growth. At the beginning gold ions are reduced and deposited as Au atoms at the edges of Ag nanoprisms (Stage 1). The Ag prism oxidation is indicated by pin–hole formation, while most Ag prisms remain (Stage 2). In Stage 3 more Au atoms are deposited, along with co-reduction of Ag^+ to form an alloy surface but with increasingly larger Au ratio. Finally, in Stage 4, the Ag@Au nanoprisms with full gold shells grow with increments in both edge length and thickness due to gold deposition on all prism facets.

possess higher surface energy than the outer prism edges and flat surface sites. Thus gold deposition occurs predominantly at the inner edges to minimize surface energy. Meanwhile, in the presence of the mild reducing agent HyA, the Ag nanoprism would act as an electron-transfer mediator to catalyze the reduction of gold ions as well as the silver ions from oxidatively etched Ag prisms to deposit on the prism surfaces. This seed-mediated deposition process can be illustrated as in Equations 4 and 5,[33] where Ag_x and Ag_xAu_y represent pure Ag nanoprisms and bimetallic nanocrystals, respectively.

$$Ag_x\ (s) + AuCl_4^-\ (aq) + 3\ e^- \rightarrow Ag_xAu\ (s) + 4Cl^-\ (aq) \quad (4)$$

$$Ag_xAu_y\ (s) + AuCl_4^-\ (aq) + 3\ e^- \rightarrow Ag_xAu_{y+1}\ (s) + 4Cl^-\ (aq)$$

$$3Ag\ (s) + AuCl_4^-\ (aq) \rightarrow Au\ (s) + 3Ag^+\ (aq) + 4Cl^-\ (aq)$$

$$Ag_xAu_y\ (s) + Ag^+\ (aq) + e^- \rightarrow Ag_{x+1}Au_y\ (s) \quad (5)$$

In fact, the Equation (4) represents a bimetallic growth towards higher atomic Au ratio, while the reaction in Equation (5) shows the possibility of co-reduction of Ag^+ ions that comes from the etching of Ag nanoprisms by the gold ions. The concurrence of these reactions leads to Ag–Au alloy deposition in the refilling process. To get a final shell of pure gold, the reaction in (4) has to be much faster than that in (5), which is achieved by appropriately increasing the reagents' infusion rate and solution pH. The characterization results indicate that by successive formation of thin bimetallic (Ag_xAu_y) shells on the Ag nanoprism surface with continuous increase of the y/x ratio, a pure gold shell will eventually form on the outermost layer of the Ag@Au nanoprisms.

iv) Further Gold Deposition on All Facets of the Prisms to Form Fully Gold-Coated Nanoprisms: After the pinholes are completely backfilled, further gold deposition takes place on all nanoprism surfaces including tips, edges, and triangular faces. From the HAADF-STEM image (**Figure 6**), we can observe that the brightness of the (111) triangular face decreases due to a thickness increment from pure gold deposition and the higher atomic number of gold than silver. The fully gold-covered Ag nanoprisms are quite stable and show excellent etching resistance to $HAuCl_4$ (Figure S3E). The morphology of these gold-coated nanoprisms remained unchanged even after six months. In addition, if the Au deposition rate is uncontrollably fast in this stage, we could observe wavy and dendritic structures (Figure S3A–S3D), which are not favored.

To better illustrate these four different stages of gold coating, a schematic diagram of the growth model from the cross-sectional view is depicted in **Scheme 2**. It should be noted that these four growth stages may overlap, particularly at the end of each stage.

3. Conclusion

In summary, we present a surfactant-free gold-coating process of Ag nanoprisms with systematic structural studies on the resulting Ag@Au core–shell nanoprisms. The results presented here are important as they demonstrate the first successful attempt to produce fully gold-coated core–shell structures from Ag nanoprism templates while maintaining the prism morphology and controllable Au shell thickness. The pure gold shell on the nanoprism surface provides strong stability against etching. TEM analyses prove that the structure is a core–shell nanoprism rather than a nanobox or nanocage. The LSPR band of the resultant core–shell prism structures could be tuned from 550 to 1100 nm by controlling the Au shell thickness. More importantly, these gold-coated nanoprisms have very clean surfaces and are free from strong binding surfactants, which endows easier and more flexible functionality for a large number of potential applications in biosensing and bioimaging.

4. Experimental Section

Synthesis of Silver Nanoparticles: In a typical synthesis, Millipore water (190 mL), $AgNO_3$ (1 mL, 30 mM), and sodium citrate (2 mL, 25 mM) were combined in a 500-mL three-necked flask. The flask was immersed in an ice bath, and the solution was bubbled with nitrogen gas under vigorous stirring for 30 minutes. $NaBH_4$ (1 mL aqueous solution, 70 mM, freshly prepared with ice-cold water) was rapidly injected into the solution. Over the next 20 min, five drops of the $NaBH_4$ solution were added into the solution every 2 min. Then 1 mL solution of bis(p-sulfonatophenyl) phenylphosphine dihydrate dipotassium (5 mM) and 1 mL $NaBH_4$ solution were added dropwise into the reaction mixture. The resulting solution of silver nanoparticles was gently stirred for 3 h in the ice bath and allowed to age overnight at about 4 °C in the dark.

Photomediated Preparation of Silver Nanoprism: In a typical experiment, the silver nanoparticle solution (20 mL) was irradiated with a halogen lamp (150 W) coupled with an optical bandpass filter centered at 600 ± 20 nm. The photoreaction was monitored by UV-Vis spectroscopy, and stopped when the major extinction band at about 700 nm showed no more obvious changes.

Synthesis of Triangular Ag@Au Nanostructure: The as-prepared Ag nanoprism solution (15 mL) was added into 20 mL of Millipore water in a glass vial placed in an ice bath, followed by infusion of ca. 2–4 mL solution of 3 mM HyA and ca. 2–4 mL solution of 0.27 mM $HAuCl_4$ into the solution through two separate tubes on a mechanical syringe pump with vigorous stirring. The infusion rate was set as 1–3 mL h^{-1}. Basic HyA solution was prepared by adding 200 μL NaOH (0.5 M) into 6 mL as-prepared HyA solution.

Sample Preparation for Electron Microscopy: Samples were prepared for electron microscopy by drying a drop of nanoprism solution on a carbon-coated copper grid or a SiO_2-supported TEM grid (Ted Pella, Inc.). For flat-lying nanoprisms, the TEM grid was pretreated with 0.1 wt% solution of polyethylenimine (PEI) prior to drying the nanoprism solution on the surface. For standing nanoprisms, the nanoprisms were resuspended in ethanol before deposition and drying on the TEM grid.

Electron Microscopic Characterization: TEM measurements were carried out on a JEOL JEM-2010 TEM or a JEM-2100F TEM at an operation voltage of 200 kV. The HAADF-STEM imaging was carried out on a FEI Titan TEM with a Schottky electron source and an operation voltage of 200 kV. STEM images were obtained by using an electron probe with an approximate diameter of 0.2 nm. EDX line-scan profiles were taken by using a probe diameter of ca. 0.5 nm with 5 s acquisition time for each spectrum.

Supporting Information

Supporting Information is available from the Wiley Online Library or from the author.

Acknowledgements

The authors acknowledge financial support from NTU Start-Up Grant (SUG), NTU Seed funding for Solar Fuels Laboratory, and CRP (NRF-CRP5-2009-04) from NRF Singapore. We also thank the Facility for Analysis, Characterization, Testing and Simulation (FACTS) at NTU for assistance, and Mr. Lai Chee Hoong Patrick and Mr. Lim Yin Koon for their kind help in equipment usage.

Received: August 26, 2011
Revised: October 4, 2011
Published online: January 9, 2012

[1] J. E. Millstone, S. J. Hurst, G. S. Métraux, J. I. Cutler, C. A. Mirkin, *Small* **2009**, *5*, 646.
[2] C. J. Murphy, T. K. Sau, A. M. Gole, C. J. Orendorff, J. Gao, L. Gou, S. E. Hunyadi, T. Li, *J. Phys. Chem. B* **2005**, *109*, 13857.
[3] B. J. Wiley, S. H. Im, Z.-Y. Li, J. McLellan, A. Siekkinen, Y. Xia, *J. Phys. Chem. B* **2006**, *110*, 15666.
[4] K. L. Kelly, E. Coronado, L. L. Zhao, G. C. Schatz, *J. Phys. Chem. B* **2003**, *107*, 668.
[5] C. Xue, X. Chen, S. J. Hurst, C. A. Mirkin, *Adv. Mater.* **2007**, *19*, 4071.
[6] S. Chen, Y. Yang, *J. Am. Chem. Soc.* **2002**, *124*, 5280.
[7] Z. J. Jiang, C. Y. Liu, L. W. Sun, *J. Phys. Chem. B* **2005**, *109*, 1730.
[8] A. L. Pyayt, B. Wiley, Y. Xia, A. Chen, L. Dalton, *Nat. Nanotechnol.* **2008**, *3*, 660.
[9] S. Peng, Y. Lee, C. Wang, H. Yin, S. Dai, S. Sun, *Nano Res.* **2008**, *1*, 229.
[10] X. J. Xie, W. Xu, T. H. Li, X. G. liu, *Small* **2011**, *7*, 1393.
[11] M. J. Mulvihill, X. Y. Ling, J. Henzie, P. Yang, *J. Am. Chem. Soc.* **2009**, *132*, 268.
[12] X. D. Chen, S. Z. Li, C. Xue, M. J. Banholzer, G. C. Chartz, C. A. Mirkin, *ACS Nano* **2009**, *3*, 87.
[13] B. Yang, N. Lu, D. Qi, R. Ma, Q. Wu, J. Hao, X. Liu, Y. Mu, V. Reboud, N. Kehagias, C. M. S. Torres, F. Y. C. Boey, X. Chen, L. Chi, *Small* **2010**, *6*, 1038.
[14] Y. Chen, K. Munechika, D. S. Ginger, *Nano Lett.* **2007**, *7*, 690.
[15] J. R. Lakowicz, *Anal. Biochem.* **2005**, *337*, 171.
[16] T. Hasobe, H. Imahori, P. V. Kamat, T. K. Ahn, S. K. Kim, D. Kim, A. Fujimoto, T. Hirakawa, S. Fukuzumi, *J. Am. Chem. Soc.* **2004**, *127*, 1216.
[17] A. P. Kulkarni, K. M. Noone, K. Munechika, S. R. Guyer, D. S. Ginger, *Nano Lett.* **2010**, *10*, 1501.
[18] X. Z. Zhou, X. Huang, X. Y. Qi, S. X. Wu, C. Xue, F. Boey, Q. Y. Yan, P. Chen, H. Zhang, *J. Phys. Chem. C* **2009**, *113*, 10842.
[19] J. Zhang, M. R. Langille, C. A. Mirkin, *Nano Lett.* **2011**, *11*, 2495.
[20] Y. G. Sun, B. Gates, B. Mayers, Y. N. Xia, *Nano Lett.* **2002**, *2*, 165.
[21] C. Xue, C. A. Mirkin, *Angew. Chem. Int. Ed.* **2007**, *119*, 2082.
[22] J. E. Millstone, G. S. Metraux, C. A. Mirkin, *Adv. Func. Mater.* **2006**, *16*, 1209.
[23] W. Niu, S. Zheng, D. Wang, X. Liu, H. Li, S. Han, J. Chen, Z. Tang, G. Xu, *J. Am. Chem. Soc.* **2008**, *131*, 697.
[24] M. R. Langille, M. L. Personick, J. Zhang, C. A. Mirkin, *J. Am. Chem. Soc.* **2011**, *133*, 10414.
[25] X. Huang, X. Qi, Y. Huang, S. Li, C. Xue, C. L. Gan, F. Boey, H. Zhang, *ACS Nano* **2010**, *4*, 6196.
[26] D. Seo, C. I. Yoo, I. S. Chung, S. M. Park, S. Ryu, H. Song, *J. Phys. Chem. C* **2008**, *112*, 2469.
[27] B. J. Wiley, Y. Xiong, Z. Y. Li, Y. Yin, Y. Xia, *Nano Lett.* **2006**, *6*, 765.
[28] L. M. Liz-Marzán, *Langmuir* **2005**, *22*, 32.
[29] C. Xue, J. E. Millstone, S. Y. Li, C. A. Mirkin, *Angew. Chem. Int. Ed.* **2007**, *46*, 8436.
[30] M. Tsuji, R. Matsuo, P. Jiang, N. Miyamae, D. Ueyama, M. Nishio, S. Hikino, H. Kumagae, K. S. N. Kamarudin, X.L. Tang, *Cryst. Growth Des.* **2008**, *8*, 2528.
[31] G. S. Metraux, Y. C. Cao, R. C. Jin, C. A. Mirkin, *Nano Lett.* **2003**, *3*, 519.
[32] D. Aherne, M. Gara, J. M. Kelly, Y. K. Gun'ko, *Adv. Func. Mater.* **2010**, *20*, 1329.
[33] X. Zou, E. Ying, S. Dong, *J. Coll. Inter. Sci.* **2007**, *306*, 307.
[34] R. G. Sanedrin, D. G. Georganopoulou, S. Park, C. A. Mirkin, *Adv. Mater.* **2005**, *17*, 1027.
[35] D. Aherne, D. E. Charles, M. E. Brennan-Fournet, J. M. Kelly, Y. K. Gun'ko, *Langmuir* **2009**, *25*, 10165.
[36] C. Novo, P. Mulvaney, *Nano Lett.* **2007**, *7*, 520.
[37] Y. Sun, Y. Xia, *J. Am. Chem. Soc.* **2004**, *126*, 3892.